

# Optical isolation induced by subwavelength spinning particle via spin-orbit interaction

Hongkang Shi,<sup>1,2</sup> Yuqiong Cheng,<sup>2</sup> Zheng Yang,<sup>2</sup> Yuntian Chen,<sup>1,3,\*</sup> and Shubo Wang<sup>2,4,†</sup>

<sup>1</sup>*School of Optical and Electronic Information, Huazhong University of Science and Technology, Wuhan 430074, China*

<sup>2</sup>*Department of Physics, City University of Hong Kong, Hong Kong, China*

<sup>3</sup>*Wuhan National Laboratory of Optoelectronics, Huazhong University of Science and Technology, Wuhan 430074, China*

<sup>4</sup>*City University of Hong Kong Shenzhen Research Institute, Shenzhen, Guangdong 518057, China*

(Dated: November 25, 2020)

Optical isolation enables nonreciprocal manipulations of light with broad applications in optical communications. Optical isolation by rotating structures has drawn considerable attention due to its magnetic-free nature and unprecedented performance. Conventional rotation-based optical isolation relies on the use of bulky cavities hindering applications in subwavelength photonics. Here, we propose a novel mechanism of optical isolation by integrating the unique dispersion of a hyperbolic metamaterial with the transverse spin-orbit interaction of evanescent waves. We show that rotation of a subwavelength hyperbolic nanoparticle breaks the time-reversal symmetry and yields two resonant chiral modes that selectively couple to the transverse spin of waveguide modes. Remarkably, the transverse spin-orbit interaction can give rise to unidirectional coupling and  $> 95\%$  isolation of infrared light at an experimentally feasible rotation speed. Our work fuses the two important fields of optical isolation and photonic spin-orbit interactions, leading to magnetic-free yet compact nonreciprocal devices for novel applications in optical communications, chiral quantum optics, and topological photonics.

**Introduction.**—Nonreciprocity, i.e., an asymmetric response under interchange of the source and observation point, can give rise to one-way transport of light and thus optical isolation, which has numerous novel applications, such as invisible sensing [1] and noise-tolerant quantum computing [2, 3]. Only a few approaches can be applied to achieve optical isolation, including nonlinearity [4–6], time modulation [7–9], and external biasing [10]. Nonlinear materials only work for high-intensity signals, while time modulation faces challenges in achieving fast and robust effects at optical frequencies [2]. The available external biasing technique routinely relies on a magnetic field, which is incompatible with on-chip optical devices due to the lack of magneto-optical materials at high frequencies. Alternatively, external biasing via structural rotation can be a promising solution to magnet-free nonreciprocal devices, as evident from the unprecedented performance of recent structural rotation-based optical isolators [11–14]. However, these designs typically employ the whispering gallery modes of bulky cavities which are unsuitable for subwavelength photonics.

In this letter, we propose a mechanism of optical isolation based on a spinning hyperbolic particle with a radius of  $\sim \lambda/5$  by taking advantage of the transverse spin-orbit interaction (SOI). Transverse SOI is a generic property of evanescent waves in various systems including waveguides [15–18] and metal surfaces [19–22]. The intrinsic locking between the transverse spin angular momentum and the direction of linear momentum allows spin-dependent control of light propagation, leading to pseudo-nonreciprocal phenomena such as unidirectional coupling for one of the spin states [3, 18]. We show that with the particle rotation, a synthetic gauge field emerges and serves as a bias to remove the spin degeneracy of the chiral modes of the particle. Consequently, the

transverse SOI in the particle-waveguide configuration can lead to truly unidirectional coupling beyond pseudo-nonreciprocity and thus optical isolation.

**Wave equation for a spinning hyperbolic particle.**—We consider a spinning particle (angular velocity of  $\Omega$ ) located above a silicon ( $\epsilon_{\text{Si}} = 11.9$ ) waveguide with a distance of  $g$ , as shown in Fig. 1. The particle has inner radius  $R_{\text{in}}$  and outer radius  $R_{\text{out}}$  and consists of multiple layers of silver and silicon with respective thicknesses of  $d_1$  and  $d_2$ , as shown in the left inset in Fig. 1. For simplicity, we take  $d_1 = d_2 = d$ . The relative permittivity of silver is described by a Drude model  $\epsilon_{\text{Ag}} = \epsilon_{\infty} - \omega_p^2/(\omega^2 + i\omega\gamma)$  with  $\epsilon_{\infty} = 3.92$ ,  $\omega_p = 1.33 \times 10^{16}$  Hz, and  $\gamma = 2.73 \times 10^{13}$  Hz [23]. We neglect material loss and consider only the real part of  $\epsilon_{\text{Ag}}$  in the numerical simulations. The multilayer structure is known as a

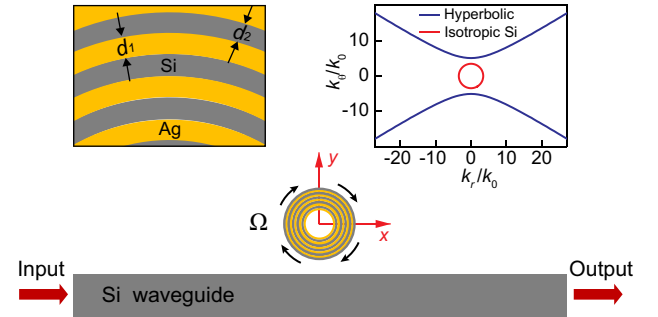


FIG. 1. Schematic of the proposed optical isolator consisting of a subwavelength spinning particle near a waveguide. The left inset shows a zoom-in of the metamaterial. The right inset shows the equifrequency lines of the effective hyperbolic medium and isotropic silicon.

hyperbolic metamaterial, which in the long-wavelength limit can be described as an effective homogeneous and anisotropic medium characterized by the dispersion relation  $k_\theta^2/\varepsilon_r - k_r^2/|\varepsilon_\theta| = \omega^2/c^2$ , where  $\varepsilon_\theta = (\varepsilon_{\text{Si}} + \varepsilon_{\text{Ag}})/2$  and  $\varepsilon_r = 2\varepsilon_{\text{Si}}\varepsilon_{\text{Ag}}/(\varepsilon_{\text{Si}} + \varepsilon_{\text{Ag}})$  are the effective permittivities along principle axes [24]. The right inset in Fig. 1 shows the equifrequency lines of the effective hyperbolic medium in comparison with that of isotropic silicon. The hyperbolic medium supports an unbounded wavevector due to its special dispersion relation [25], which is essential in realizing the subwavelength optical isolator.

Under the effective medium description, the electromagnetic properties of the spinning particle are governed by the Minkowski constitutive relations [26]:  $\mathbf{D} + \mathbf{v} \times \mathbf{H}/c^2 = \varepsilon(\mathbf{E} + \mathbf{v} \times \mathbf{B})$ ,  $\mathbf{B} + \mathbf{E} \times \mathbf{v}/c^2 = \mu(\mathbf{H} + \mathbf{D} \times \mathbf{v})$ , where  $\varepsilon$  and  $\mu$  are the effective permittivity and permeability tensors,  $c$  is the speed of light, and  $\mathbf{v}$  is the linear velocity of the material. For the considered particle,  $\varepsilon$  and  $\mu$  have only diagonal elements  $\{\varepsilon_r\varepsilon_0, \varepsilon_\theta\varepsilon_0, \varepsilon_z\varepsilon_0\}$  and  $\{\mu_0, \mu_0, \mu_0\}$ , respectively. The constitutive relations can be packed into matrix form  $\begin{bmatrix} \mathbf{D} \\ \mathbf{B} \end{bmatrix} = \begin{bmatrix} \bar{\varepsilon} & \bar{\chi}_{\text{em}} \\ \bar{\chi}_{\text{me}} & \bar{\mu} \end{bmatrix} \begin{bmatrix} \mathbf{E} \\ \mathbf{H} \end{bmatrix}$ , which is the well-known constitutive relation for bi-anisotropic media; i.e., rotation transforms the original anisotropic medium into a bi-anisotropic medium. In conventional bi-anisotropic media with reciprocity, we have  $\bar{\varepsilon} = \bar{\varepsilon}^T$ ,  $\bar{\mu} = \bar{\mu}^T$ , and  $\bar{\chi}_{\text{em}} = (\bar{\chi}_{\text{me}}^*)^T = -\bar{\chi}_{\text{me}}^T$ , corresponding to Pasteur media [27]. Here T and \* denote the transpose and the complex conjugate, respectively. However, for the spinning hyperbolic particle, we have  $\bar{\varepsilon} = \bar{\varepsilon}^T$ ,  $\bar{\mu} = \bar{\mu}^T$ , and  $\bar{\chi}_{\text{em}} = (\bar{\chi}_{\text{me}}^*)^T = \bar{\chi}_{\text{me}}^T$  [28], corresponding to Tellegen media that break time-reversal symmetry and reciprocity [27]. Using the constitutive relations, the TM-polarized Helmholtz equation can be expressed as

$$\left(\frac{1}{r} \frac{\partial}{\partial \theta} + ik_0 A_\theta\right)^2 H_z + \frac{\varepsilon'_r}{\varepsilon'_\theta} \frac{1}{r} \frac{\partial}{\partial r} \left(r \frac{\partial}{\partial r} H_z\right) + k_0^2 \varepsilon'_r \mu' H_z = 0, \quad (1)$$

where  $\varepsilon'_r = \varepsilon_r(\Lambda^2 - 1)/(\varepsilon_r\Lambda^2 - 1)$ ,  $\varepsilon'_\theta = \varepsilon_\theta$ ,  $\mu' = (\Lambda^2 - 1)/(\varepsilon_r\Lambda^2 - 1)$ ,  $A_\theta = \Lambda(1 - \varepsilon_r)/(\varepsilon_r\Lambda^2 - 1)$ ,  $\Lambda = r\Omega/c$  is the normalized rotation speed, and  $k_0$  is the wavevector in vacuum [28]. Notably, an additional term  $ik_0 A_\theta$  emerges and corresponds to a synthetic gauge field  $\mathbf{A} = A_\theta \hat{\theta}$  arising from rotation of the particle.

**Frequency splitting.**—Equation (1) allows solutions of the form  $H_z = H_z(r)e^{\pm im\theta}$ , where  $m$  is a positive integer that denotes the azimuthal quantum number. The solutions with  $\pm m$  represent a pair of chiral modes circulating in counterclockwise and clockwise directions. In the static limit (i.e.,  $\Omega = 0$ ), the synthetic gauge field  $\mathbf{A}$  vanishes, and the two modes are degenerate and orthogonal due to the time-reversal symmetry. Figure 2(a) and 2(b) show the chiral mode with  $m = +16$  in the static metamaterial particle and the corresponding effective-medium

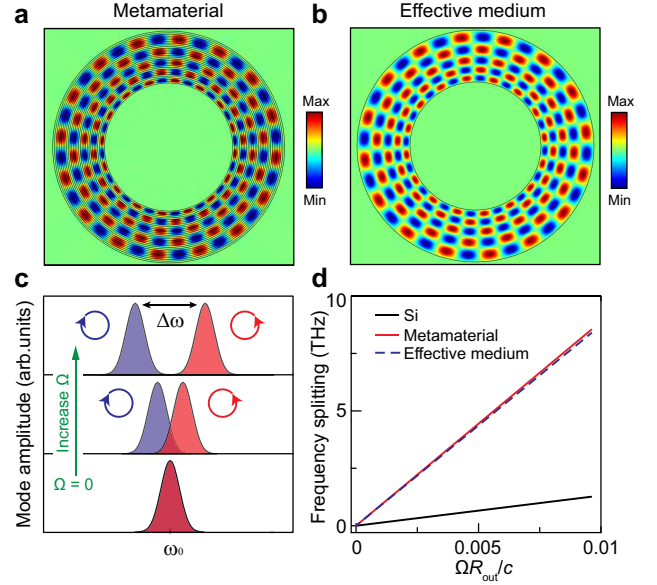


FIG. 2. Chiral mode of (a) the hyperbolic metamaterial particle and (b) the effective-medium particle. (c) Schematic showing the frequency splitting induced by rotation. (d) Comparison of frequency splitting between the hyperbolic particle and a normal silicon particle.

particle at  $f = 174.33$  THz, which are obtained via full-wave simulations using COMSOL [29]. We set  $R_{\text{in}} = 185$  nm,  $R_{\text{out}} = 335$  nm, and  $d = 5$  nm (corresponding to a size of  $R_{\text{out}} \approx \lambda/5$ ). We note that the  $H_z$  fields of the two systems agree well, demonstrating the validity of the effective-medium description.

At nonzero rotation speed (i.e.,  $\Omega \neq 0$ ), the synthetic gauge field  $\mathbf{A}$  breaks the time-reversal symmetry and removes the degeneracy of the chiral modes, which can be considered a photonic analog of the Zeeman effect. This leads to a frequency splitting  $\Delta\omega$  of the two modes. By inserting  $H_z = H_z(r)e^{\pm im\theta}$  into Eq. (1), we obtain  $\Delta\omega = 2mA_\theta c/[r(\varepsilon'_r\mu' - A_\theta^2)]$  [30]. Under the condition  $\Lambda(R_{\text{out}}) = R_{\text{out}}\Omega/c \ll 1$ , the higher-order terms with respect to  $\Lambda$  can be neglected, and we obtain  $\Delta\omega \approx 2m\Omega(1 - 1/\varepsilon_r)$ . Evidently,  $\Delta\omega$  is proportional to the rotation angular velocity  $\Omega$ . Figure 2(c) schematically shows the evolution of the chiral modes as  $\Omega$  increases. The arrowed circles indicate the circulating direction of the mode field pattern. The two modes have identical spectra at  $\Omega = 0$  but are separated at  $\Omega \neq 0$ . In addition,  $\Delta\omega$  is proportional to the azimuthal quantum number  $m$ . Thus, modes with larger  $m$  have larger  $\Delta\omega$  at the same rotation speed, which is critical to the realization of optical isolation. Such modes are absent in conventional subwavelength optical structures due to low dielectric constants. Fortunately, they can emerge in the hyperbolic particle due to the unbounded wavevector. To see the large frequency splitting of the hyperbolic particle, we compare it with that of a silicon particle, both of

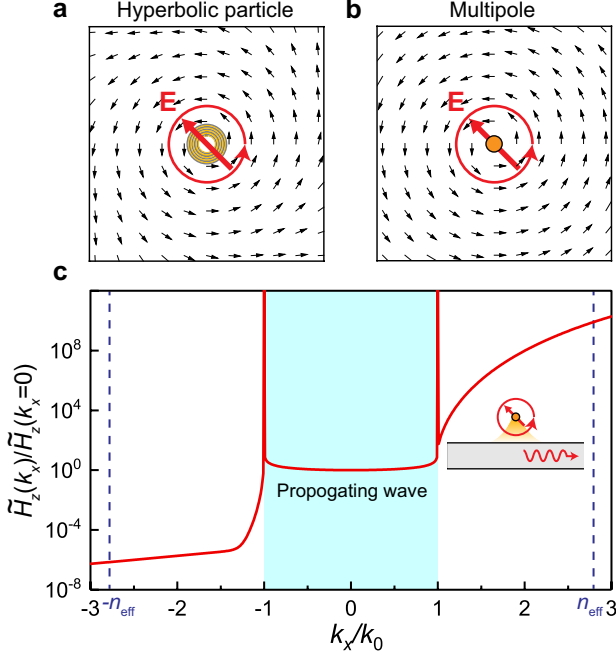


FIG. 3. Poynting vectors in (a) the chiral mode of the hyperbolic particle and (b) the corresponding multipole with  $m = 16$ . The red arrows denote the average electric field vector, and the arrowed circles show the circulating direction of the electric field (i.e., spin). (c) Normalized spectral amplitude of the  $H_z$  field for the multipole in panel (b). The inset schematically shows the unidirectional coupling under transverse spin-momentum locking.

which share the same geometric parameters and rotation speed. At  $f = 152$  THz, the silicon particle supports a pair of magnetic dipole resonances, while the hyperbolic particle supports a pair of chiral modes with  $m = \pm 8$ . Their frequency splittings are shown in Fig. 2(d) as the solid black and red lines, respectively, which are numerically computed using COMSOL. Evidently, the hyperbolic particle yields much larger frequency splitting due to the larger value of  $m$ . The dashed blue line denotes the analytical result based on effective-medium description, which agrees well with the numerical result of the meta-material particle. We note that in the case of Fig. 2(a) with  $m = \pm 16$ , the frequency splitting of the hyperbolic particle is even larger, while the counterpart modes are missing in the silicon particle due to cutoff frequencies.

*Transverse spin-orbit interaction.*—The chiral modes of the particle carry spin in the  $z$  direction (i.e., transverse spin), which can be characterized by the Stokes parameter  $S_3$  of the average electric field. The sign of  $S_3$  has a one-to-one correspondence with the circulating direction of chiral modes, i.e.,  $S_3 = 1$  ( $S_3 = -1$ ) for the mode with  $m > 0$  ( $m < 0$ ), and thus can be used to label the chiral modes  $\psi_p^\pm$  and the eigenfrequencies  $\omega_\pm$ .

By applying multipole expansions based on vector harmonics [31], we found that the field of  $\psi_p^\pm$  is approxi-

mately equivalent to that of an electromagnetic multipole [30]. Thus, the hyperbolic particle can be considered a passive point multipole due to its subwavelength nature (i.e.,  $R_{\text{out}} \approx \lambda/5$ ). For the chiral mode in Fig. 2(a), the field is equivalent to a multipole with  $m = +16$ . Figure 3(a) and 3(b) show the spin and Poynting vectors of  $\psi_p^\pm$  and the corresponding multipole, respectively. The red arrows denote the average electric field of the particle, and the arrowed circles show the circulating direction of the electric field (i.e., spin), which is the same as the circulating direction of the mode field pattern in Fig. 2(a). Notably, the Poynting vectors also circulate counterclockwise, which indicates asymmetric propagation of the near field. This can be understood with the angular spectrum representation of  $H_z$  field of the multipole [32, 33]:  $H_z(x, y) = \int_{-\infty}^{\infty} \tilde{H}_z(k_x, y) e^{ik_x x} dk_x$ ,  $\tilde{H}_z(k_x, y) = \frac{1}{2\pi} \int_{-\infty}^{\infty} H_z(x, y) e^{-ik_x x} dx$ . For the spectral component at the position of the waveguide ( $y = -g$ ), the normalized amplitude  $\tilde{H}_z(k_x)/\tilde{H}_z(k_x=0)$  with  $k_x \in [-3k_0, 3k_0]$  is shown in Fig. 3(c) as the solid red line. The shaded region corresponds to the propagating waves with  $k_x/k_0 \leq 1$ . For evanescent waves with  $k_x/k_0 \geq 1$ , the spectral amplitude unambiguously shows asymmetry with respect to  $+k_x$  and  $-k_x$ . The effective refractive index of the fundamental TM mode of the Si waveguide is  $n_{\text{eff}} = 2.77$ , as marked by the dashed blue lines in Fig. 3(c). The spectral amplitude with  $k_x = n_{\text{eff}}k_0$  is more than ten orders of magnitude larger than that of  $k_x = -n_{\text{eff}}k_0$ . Thus, the evanescent waves of the multipole couple unidirectionally to the waveguide mode, as shown by the inset in Fig. 3(c), indicating locking between the transverse spin and the direction of linear momentum  $k_x$ . Notably, such high-efficiency and spatially broadband near-field unidirectionality can only be achieved with high-order multipoles [34]. It serves as another critical element of optical isolation in our settings.

*Optical isolation.*—We now consider the particle-waveguide configuration in Fig. 1 and demonstrate the optical isolation. The waveguide thickness is 400 nm. The particle locates at  $g = 338$  nm above the waveguide and has a spinning frequency of  $\Omega/(2\pi) = 0.19$  GHz. The transmission of the fundamental TM waveguide mode is shown in Fig. 4(a), where the solid red (blue) line denotes the excitation from the left (right) input. Both transmissions have a dip corresponding to one of the chiral modes, and the two dips are spectrally separated due to the frequency splitting effect. The arrowed circles denote the spin of the chiral modes. The large transmission contrast between the “left” and “right” excitations unambiguously shows the nonreciprocity of the system, which can be applied to realize optical isolation. The isolation ratio (i.e., the absolute difference between the blue and red lines) is shown as the dashed black line in Fig. 4(a). Remarkably, large isolation ratios occur at the two eigenfrequencies of the chiral modes (i.e.,  $\omega_\pm$ ).

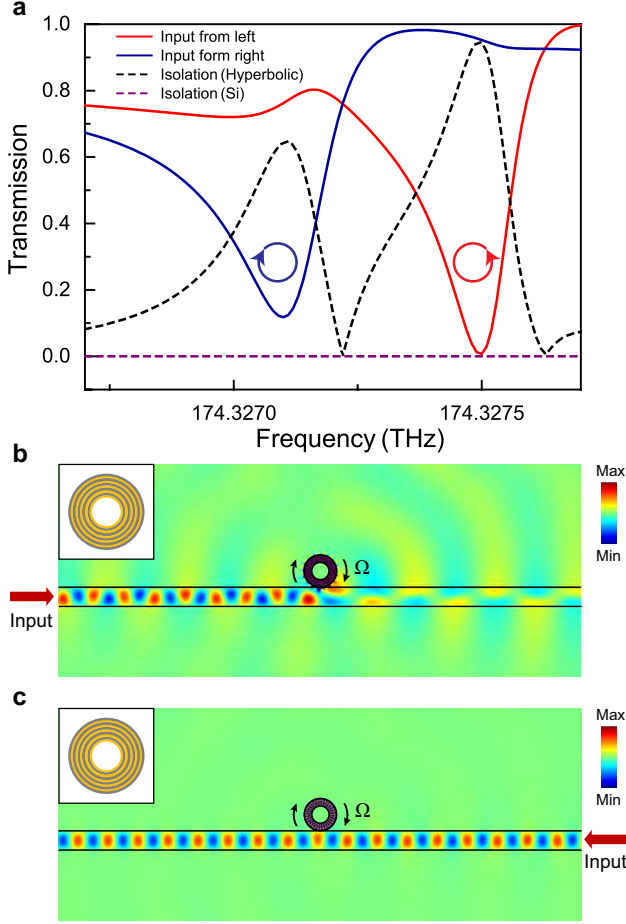


FIG. 4. (a) Transmission under the excitation of left/right input of the waveguide. (b)  $H_z$  field under the left input, showing a vanished transmission field. The residual field on the right side of the particle is attributed to the scattering of the particle. (c)  $H_z$  field under the right input.

In particular, an isolation ratio of  $> 95\%$  is achieved at  $\omega_+$ . In contrast, the isolation ratio induced by a normal silicon particle with the same size and spinning frequency (dashed purple line in Fig. 4(a)) is negligible due to the absence of any resonance in the considered subwavelength regime [30]. Figure 4(b) and 4(c) show the  $H_z$  field under opposite excitations at  $\omega_+$ . As seen, light is almost completely blocked for excitation from the left input (the field outside the waveguide is attributed to the scattering of the particle). In contrast, light can largely propagate through the waveguide when excited from the right input. The optical isolation is robust against variations in the systems geometric parameters. Another design with  $R_{\text{in}} = 370$  nm,  $R_{\text{out}} = 670$  nm and  $d = 10$  nm is provided in the Supplemental Material [30], giving  $> 94\%$  optical isolation at  $f = 150.30$  THz ( $R_{\text{out}} \approx \lambda/3$ ).

The optical isolation can be understood as a result of mode coupling under transverse spin-orbit interaction mediated by the spinning particle. The transmitted wave

can be expressed as [30]

$$\psi_{\text{out}}(\omega) = \psi_{\text{wg}}^{\pm} + \psi_{\text{wg}}^{+} C_{\pm}(\omega) \mathcal{F}(\psi_{\text{p}}^{\pm})|_{k_x = n_{\text{eff}} k_0} + \psi_{\text{wg}}^{-} C_{\pm}(\omega) \mathcal{F}(\psi_{\text{p}}^{\pm})|_{k_x = -n_{\text{eff}} k_0}, \quad (2)$$

where  $\psi_{\text{wg}}^{\pm}(x, y) = \phi_{\pm}(y)e^{\pm i n_{\text{eff}} k_0 x}$  is the waveguide mode with unit amplitude. We note that the spin sign (i.e., subscript/superscript  $\pm$ ) is locked to the propagating direction of the guided wave. Here,  $C_{\pm}(\omega) = \psi_{\text{wg}}^{\pm}(0, 0) (\bar{\psi}_{\text{p}}^{\pm})^* A / (\omega^2 - \omega_{\pm}^2 - i\gamma_{\pm})$  is the amplitude of the chiral modes excited by the guided wave,  $\bar{\psi}_{\text{p}}^{\pm}$  is the average field of the particle,  $A$  is the mode volume, and  $\gamma_{\pm}$  is the damping. Notably, the amplitude  $C_{\pm}(\omega)$  is determined by the projection of the local spin of the waveguide field onto the spin of the particle's average field, in contrast to conventional rotation-based optical isolation which depends on both spin and orbital angular momentum [30].  $\mathcal{F}(\psi_{\text{p}}^{\pm})|_{k_x = \pm n_{\text{eff}} k_0} = \tilde{H}_z(k_x = \pm n_{\text{eff}} k_0)$  is the Fourier spectral amplitude of the particle's field for  $k_x = \pm n_{\text{eff}} k_0$  at the position of the waveguide. The first term in Eq. (2) corresponds to the input wave. The second and third terms correspond to the guided waves propagating in  $+x$  and  $-x$  directions, respectively, which are coupled from the evanescent waves of  $\psi_{\text{p}}^{\pm}$ . For input from the left, the guided wave carries a positive spin ( $S_3 = +1$ ), and the upper branch of  $\pm$  should be adopted in Eq. (2). According to the result in Fig. 3(c), we have  $\mathcal{F}(\psi_{\text{p}}^{+})|_{k_x = n_{\text{eff}} k_0} \gg \mathcal{F}(\psi_{\text{p}}^{+})|_{k_x = -n_{\text{eff}} k_0}$ , i.e., the evanescent waves of the particle are coupled to the waveguide mode propagating unidirectionally to the right side [30]. Thus, the third term is negligible, and the output wave is reduced to  $\psi_{\text{L} \rightarrow \text{R}}(\omega) \approx \psi_{\text{wg}}^{+} [1 + C_{+}(\omega) \mathcal{F}(\psi_{\text{p}}^{+})|_{k_x = n_{\text{eff}} k_0}]$ . In the case that  $\gamma_{+}$  is small,  $C_{+}(\omega)$  is significantly enhanced at  $\omega = \omega_{+}$ , thus, the output wave can vanish due to the destructive interference of the two terms inside the bracket. For input from the right, the output wave is reduced to  $\psi_{\text{R} \rightarrow \text{L}}(\omega) \approx \psi_{\text{wg}}^{-} [1 + C_{-}(\omega) \mathcal{F}(\psi_{\text{p}}^{-})|_{k_x = -n_{\text{eff}} k_0}]$ . Since  $\mathcal{F}(\psi_{\text{p}}^{-})|_{k_x = -n_{\text{eff}} k_0} \approx \mathcal{F}(\psi_{\text{p}}^{+})|_{k_x = n_{\text{eff}} k_0}$  and  $C_{-}(\omega_{+}) \ll C_{+}(\omega_{+})$  due to the off-resonance of  $C_{-}(\omega)$  at  $\omega = \omega_{+}$ , the isolation ratio  $I(\omega) = |\psi_{\text{L} \rightarrow \text{R}}(\omega)|^2 - |\psi_{\text{R} \rightarrow \text{L}}(\omega)|^2$  reaches a maximum at  $\omega = \omega_{+}$ , corresponding to the second peak in Fig. 4(a). Similar analysis also applies to the peak at  $\omega = \omega_{-}$ . Note that  $I(\omega_{-}) \neq I(\omega_{+})$  because rotation breaks the mirror symmetry.

*Discussion and conclusion.*—Optical isolation by rotating structures relies on three critical elements: high rotation speed, resonance modes with a large azimuthal quantum number and a high Q factor. The three elements normally compromise each other: a high rotation speed can only be achieved for small structures which normally do not support the required resonance modes in the subwavelength regime. Thus, conventional rotation-based optical isolators typically have large volumes. Our



system shoots three birds with one stone: the hyperbolic particle is geometrically small ( $R_{\text{out}} \approx \lambda/5$ ) and supports chiral modes with a large azimuthal quantum number and a high  $Q$  factor. To realize the optical isolation, a spinning frequency of 0.19 GHz is desired. This can be achieved by using the optical tweezers technique [35–37], where a high vacuum environment combined with the approach of active parametric feedback could be applied to reduce the mechanical instability of the particle [38]. Another practical problem is material loss, which occurs in almost all metamaterials and can be solved by adding gain into the system [39–41].

As a concluding remark, optical isolation can be achieved with the spinning hyperbolic particle coupled to a waveguide via the transverse spin-orbit interaction. Our study thus paves a critical step towards on-chip optical isolation and may trigger further explorations of structural rotation-induced effects and phenomena, such as the nonreciprocal hopping in periodic structures and the non-Hermiticity due to asymmetric couplings. In addition, the small size of the optical insulator is perfect for integration with compact optical circuits, which can generate novel applications in optical communications, chiral quantum optics, and topological photonics.

The work described in this paper was supported by grants from the Research Grants Council of the Hong Kong Special Administrative Region, China [Project No. CityU 11301820] and the National Natural Science Foundation of China (No. 11904306 and No. 11874026).

---

\* yuntian@hust.edu.cn

† shubwang@cityu.edu.hk

- [1] H. Dutton, *Understanding Optical Communications* (Prentice Hall, New Jersey, 1998).
- [2] D. L. Sounas and A. Al, *Nat. Photon.* **11**, 774 (2017).
- [3] P. Lodahl, S. Mahmoodian, S. Stobbe, A. Rauschenbeutel, P. Schneeweiss, J. Volz, H. Pichler, and P. Zoller, *Nature* **541**, 473 (2017).
- [4] L. Fan, J. Wang, L. T. Varghese, H. Shen, B. Niu, Y. Xuan, A. M. Weiner, and M. Qi, *Science* **335**, 447 (2012).
- [5] B. Peng, K. Zdemir, F. Lei, F. Monifi, M. Gianfreda, G. L. Long, S. Fan, F. Nori, C. M. Bender, and L. Yang, *Nat. Phys.* **10**, 394 (2014).
- [6] L. Chang, X. Jiang, S. Hua, C. Yang, J. Wen, L. Jiang, G. Li, G. Wang, and M. Xiao, *Nat. Photon.* **8**, 524 (2014).
- [7] Z. Yu and S. Fan, *Nat. Photon.* **3**, 91 (2009).
- [8] D. L. Sounas, C. Caloz, and A. Al, *Nat. Commun.* **4**, 2407 (2013).
- [9] N. A. Estep, D. L. Sounas, J. Soric, and A. Al, *Nat. Phys.* **10**, 923 (2014).
- [10] H. B. G. Casimir, *Rev. Mod. Phys.* **17**, 343 (1945).
- [11] S. Maayani, R. Dahan, Y. Kligerman, E. Moses, A. U. Hassan, H. Jing, F. Nori, D. N. Christodoulides, and T. Carmon, *Nature* **558**, 569 (2018).
- [12] R. Huang, A. Miranowicz, J.-Q. Liao, F. Nori, and H. Jing, *Phys. Rev. Lett.* **121**, 153601 (2018).
- [13] H. Zhang, R. Huang, S.-D. Zhang, Y. Li, C.-W. Qiu, F. Nori, and H. Jing, *Nano Lett.* **20**, 7594 (2020).
- [14] Y.-F. Jiao, S.-D. Zhang, Y.-L. Zhang, A. Miranowicz, L.-M. Kuang, and H. Jing, *Phys. Rev. Lett.* **125**, 143605 (2020).
- [15] J. Petersen, J. Volz, and A. Rauschenbeutel, *Science* **346**, 67 (2014).
- [16] B. le Feber, N. Rotenberg, and L. Kuipers, *Nat. Commun.* **6**, 6695 (2015).
- [17] A. B. Young, A. C. T. Thijssen, D. M. Beggs, P. Androvitsaneas, L. Kuipers, J. G. Rarity, S. Hughes, and R. Oulton, *Phys. Rev. Lett.* **115**, 153901 (2015).
- [18] S. Wang, B. Hou, W. Lu, Y. Chen, Z. Q. Zhang, and C. T. Chan, *Nat. Commun.* **10**, 832 (2019).
- [19] F. J. Rodriguez-Fortuo, G. Marino, P. Ginzburg, D. O'Connor, A. Martinez, G. A. Wurtz, and A. V. Zayats, *Science* **340**, 328 (2013).
- [20] K. Y. Bliokh, A. Y. Bekshaev, and F. Nori, *Nat. Commun.* **5**, 3300 (2014).
- [21] S. B. Wang and C. T. Chan, *Nat. Commun.* **5**, 3307 (2014).
- [22] D. O'Connor, P. Ginzburg, F. J. Rodriguez-Fortuo, G. A. Wurtz, and A. V. Zayats, *Nat. Commun.* **5**, 5327 (2014).
- [23] Q. H. Song and H. Cao, *Phys. Rev. Lett.* **105**, 053902 (2010).
- [24] A. Poddubny, I. Iorsh, P. Belov, and Y. Kivshar, *Nat. Photon.* **7**, 948 (2013).
- [25] X. Yang, J. Yao, J. Rho, X. Yin, and X. Zhang, *Nat. Photon.* **6**, 450 (2012).
- [26] H. Minkowski, *Ges. Wiss. Göttingen, Math.-Phys. Kl.* **2**, 53 (1908).
- [27] A. H. Sihvola, A. J. Viitanen, I. V. Lindell, and S. A. Tretyakov, *Electromagnetic Waves in Chiral and Bi-Isotropic Media* (Artech House, Boston, 1994).
- [28] H. Shi, Z. Xiong, W. Chen, J. Xu, S. Wang, and Y. Chen, *Opt. Express* **27**, 28114 (2019).
- [29] [www.comsol.com](http://www.comsol.com).
- [30] Supplemental material.
- [31] C. F. Bohren and D. R. Huffman, *Absorption and Scattering of Light by Small Particles* (Wiley-VCH, New York, 1998).
- [32] R. Borghi, *J. Opt. Soc. Am. A* **21**, 1805 (2004).
- [33] L. Novotny and B. Hecht, *Principles of Nano-Optics* (Cambridge University Press, New York, 2012).
- [34] J. E. Vázquez-Lozano, A. Martínez, and F. J. Rodríguez-Fortuo, *Phys. Rev. Applied* **12**, 024065 (2019).
- [35] R. Reimann, M. Doderer, E. Hebestreit, R. Diehl, M. Frimmer, D. Windey, F. Tebbenjohanns, and L. Novotny, *Phys. Rev. Lett.* **121**, 033602 (2018).
- [36] J. Ahn, Z. Xu, J. Bang, Y.-H. Deng, T. M. Hoang, Q. Han, R.-M. Ma, and T. Li, *Phys. Rev. Lett.* **121**, 033603 (2018).
- [37] J. Ahn, Z. Xu, J. Bang, P. Ju, X. Gao, and T. Li, *Nat. Nanotechnol.* **15**, 89 (2020).
- [38] J. Gieseler, B. Deutsch, R. Quidant, and L. Novotny, *Phys. Rev. Lett.* **109**, 103603 (2012).
- [39] H. Rong, A. Liu, R. Jones, O. Cohen, D. Hak, R. Nicolaescu, A. Fang, and M. Paniccia, *Nature* **433**, 292 (2005).
- [40] M. I. Stockman, *Opt. Express* **19**, 22029 (2011).
- [41] J. B. Khurgin, *Nat. Nanotechnol.* **10**, 2 (2015).